

PARALLEL HIGHER-ORDER FINITE ELEMENT METHOD FOR ACCURATE FIELD COMPUTATIONS IN WAKEFIELD AND PIC SIMULATIONS

A. Candel*, A. Kabel, L. Lee, Z. Li, C. Limborg, C. Ng,
E. Prudencio, G. Schussman, R. Uplenchwar and K. Ko,
SLAC, Menlo Park, CA 94025, U. S. A.

Abstract

Over the past years, SLAC's Advanced Computations Department (ACD), under SciDAC sponsorship, has developed a suite of 3D (2D) parallel higher-order finite element (FE) codes, T3P (T2P) and Pic3P (Pic2P), aimed at accurate, large-scale simulation of wakefields and particle-field interactions in radio-frequency (RF) cavities of complex shape. The codes are built on the FE infrastructure that supports SLAC's frequency domain codes, Omega3P and S3P, to utilize conformal tetrahedral (triangular) meshes, higher-order basis functions and quadratic geometry approximation. For time integration, they adopt an unconditionally stable implicit scheme. Pic3P (Pic2P) extends T3P (T2P) to treat charged-particle dynamics self-consistently using the PIC (particle-in-cell) approach, the first such implementation on a conformal, unstructured grid using Whitney basis functions. Examples from applications to the International Linear Collider (ILC), Positron Electron Project-II (PEP-II), Linac Coherent Light Source (LCLS) and other accelerators will be presented to compare the accuracy and computational efficiency of these codes versus their counterparts using structured grids.

INTRODUCTION

The Office of Science in the U. S. DOE is promoting the use of High Performance Computing (HPC) in projects relevant to its mission via the 'Scientific Discovery through Advanced Computing' (SciDAC) program which began in 2001 [1]. Since 1996, SLAC has been developing a parallel accelerator modeling capability, first under the DOE Grand Challenge and now under SciDAC, for use on HPC platforms to enable the large-scale electromagnetic simulations needed for improving existing facilities and optimizing the design of future machines.

FINITE ELEMENT MAXWELL TIME-DOMAIN

A short introduction to the employed finite element method for simulating Maxwell's equations in time domain is given in the following.

Vector Wave Equation

Both Maxwell's curl equations (Ampere's and Faraday's laws) can be combined to yield the (loss-less) inhomogeneous vector wave equation for the electric field:

$$\epsilon \frac{\partial^2}{\partial t^2} \mathbf{E} + \nabla \times \mu^{-1} \nabla \times \mathbf{E} = -\frac{\partial}{\partial t} \mathbf{J}. \quad (1)$$

It can be integrated in time, similar to [2], to obtain

$$\epsilon \frac{\partial^2}{\partial t^2} \int_{-\infty}^t \mathbf{E} d\tau + \nabla \times \mu^{-1} \nabla \times \int_{-\infty}^t \mathbf{E} d\tau = -\mathbf{J}, \quad (2)$$

where \mathbf{E} is the electric field intensity, \mathbf{J} is the electric current source density, and ϵ and μ are the electric permittivity and magnetic permeability.

Spatial Discretization

$\int_{-\infty}^t \mathbf{E} d\tau$ in Eq. (2) can be decomposed into a chosen set of spatially fixed finite element basis functions $\mathbf{N}_i(\mathbf{x})$ with time-dependent coefficient vector $\mathbf{e}(t)$:

$$\int_{-\infty}^t \mathbf{E}(\mathbf{x}, \tau) d\tau = \sum_i \mathbf{e}_i(t) \cdot \mathbf{N}_i(\mathbf{x}). \quad (3)$$

The degrees of freedom (DOF's) of the system are given

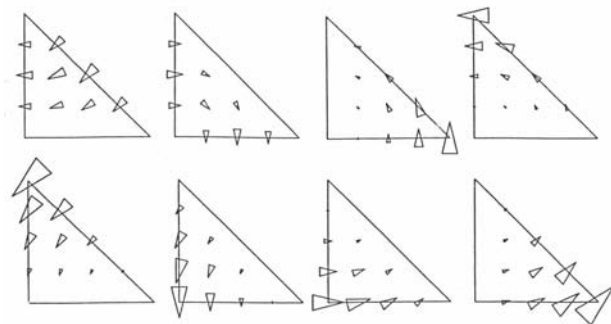


Figure 1: Unit elements with second-order Whitney vector basis functions in 2D.

by the coefficients. In our approach, Whitney basis functions are used; an illustration of second-order Whitney basis functions in 2D is shown in Fig. 1. A second-order conformal boundary approximation is obtained by using

*candel@slac.stanford.edu

quadratic transformations to map the unit elements onto their counterparts in real space.

Substituting Eq. (3) into Eq. (2), multiplying by a test function and integrating over the computational domain Ω results in the following matrix equation:

$$[\mathbf{T}] \frac{\partial^2 \mathbf{e}}{\partial t^2} + [\mathbf{R}] \frac{\partial \mathbf{e}}{\partial t} + [\mathbf{S}] \mathbf{e} = \mathbf{f}, \quad (4)$$

with the so-called mass and stiffness matrices $[\mathbf{T}]$ and $[\mathbf{S}]$:

$$[\mathbf{T}]_{ij} = \int_{\Omega} \epsilon \mathbf{N}_i \cdot \mathbf{N}_j \, d\Omega, \quad (5)$$

$$[\mathbf{S}]_{ij} = \int_{\Omega} \mu^{-1} \nabla \times \mathbf{N}_i \cdot \nabla \times \mathbf{N}_j \, d\Omega, \quad (6)$$

while the damping matrix $[\mathbf{R}]$ accounts for any open (absorbing) boundary conditions on the surface $\partial\Omega$ of the computational domain:

$$[\mathbf{R}]_{ij} = \frac{1}{c} \int_{\partial\Omega} \hat{\mathbf{n}} \times \mathbf{N}_i \cdot \hat{\mathbf{n}} \times \mathbf{N}_j \, dS, \quad (7)$$

with surface normal $\hat{\mathbf{n}}$. Lossy materials lead to additional terms and are not considered here for simplicity.

Temporal Discretization

The time evolution of $\mathbf{e}(t)$, starting from proper initial conditions, is obtained by integrating Eq. (4) over time with the unconditionally stable implicit Newmark-Beta scheme [3], which has been extended to allow for arbitrarily changing time steps. A sparse linear system needs to be solved at every time step. The electric field \mathbf{E}^n and the magnetic flux density \mathbf{B}^n at the n^{th} time step are then easily obtained from the solution vector \mathbf{e}^n as follows:

$$\mathbf{E}^n(\mathbf{x}) = \sum_i (\partial_t \mathbf{e}^n)_i \cdot \mathbf{N}_i(\mathbf{x}) \quad (8)$$

and

$$\mathbf{B}^n(\mathbf{x}) = - \sum_i (\mathbf{e}^n)_i \cdot \nabla \times \mathbf{N}_i(\mathbf{x}) \quad (9)$$

by using Faraday's law. A second-order approximation of $\partial_t \mathbf{e}^n$ is obtained by fitting a parabola through the last three time steps $\{\mathbf{e}^{n-2}, \mathbf{e}^{n-1}, \mathbf{e}^n\}$ and evaluating its time derivative at the last point in time.

Field Excitation

The system (4) is driven by the right-hand-side $\mathbf{f} = \mathbf{f}_{\text{BC}} + \mathbf{f}_{\text{J}}$, given by boundary conditions and current sources inside the computational domain, that is,

$$[\mathbf{f}_{\text{J}}]_i = - \int \mathbf{N}_i \cdot \mathbf{J} \, d\Omega. \quad (10)$$

For wakefield calculations, where a rigid beam is assumed to be traveling at the speed of light, the electric current density distribution can be calculated analytically from the given particle distribution.

For non-relativistic velocities, space charge forces act back on the particle bunch and need to be determined self-consistently from the particle-field interaction. The particle-in-cell (PIC) method is used to numerically model the particle-field interaction and is outlined in the following.

Particle-In-Cell Method

Numerical charge conservation is of utmost importance in all PIC methods where current \mathbf{J} and charge ρ densities are deposited on the computational grid. It is commonly obtained by enforcing the discrete analog of the continuity equation

$$\frac{\partial \rho}{\partial t} + \nabla \cdot \mathbf{J} = 0 \quad (11)$$

rigorously, after ensuring that the initial conditions fulfill the discrete analogs of the two Maxwell's divergence equations $\nabla \cdot \mathbf{B} = 0$ and $\nabla \cdot \mathbf{E} = \rho$. The particle distribution is modeled by a number of macro particles specified by position \mathbf{x} , momentum \mathbf{p} , rest mass m and charge q attributes. The total current density is then approximated as

$$\mathbf{J}(\mathbf{x}, t) = \sum_i q_i \cdot \mathbf{v}_i(t) \cdot \delta(\mathbf{x} - \mathbf{x}_i), \quad (12)$$

with $\mathbf{v} = \frac{\mathbf{p}}{\gamma m}$ and $\gamma = \sqrt{1 + |\mathbf{p}|^2/m^2 c^2}$. Note that numerical charge conservation is contingent upon accurately integrating Eq. (10), which can be done very efficiently using Gaussian quadrature rules.

The macro particles obey the classical relativistic collision-less (Newton-Lorentz) equations of motion,

$$\frac{d\mathbf{r}}{dt} = \mathbf{v}, \quad (13)$$

$$\frac{d\mathbf{p}}{dt} = q(\mathbf{E} + \mathbf{v} \times \mathbf{B}), \quad (14)$$

which are integrated using the standard 'Boris' pusher, an explicit method splitting the momentum update into two electric accelerations and an intermediate magnetic rotation [4]. For simplicity, the same time step is used for the field solver and for the particle pusher. This is reasonable when space charge effects are significant, especially since the electromagnetic fields are readily available, cf. Eqs. (8) and (9).

Note that, since the finite element basis functions are properly defined everywhere in the domain, interpolations are not necessary in either the scattering of current density or the gathering of the electromagnetic fields. Furthermore, an increase in the polynomial order of the finite element basis functions naturally leads to higher-order accurate, self-consistent particle-field coupling. Achieving charge conservation in this way is equivalent to, but much less laborious than, using complicated higher-order interpolation schemes commonly found in finite-difference codes [5].

THE TIME-DOMAIN CODES

Based on the methods outlined above, several parallel finite element Maxwell time domain codes have been developed under the U. S. DOE SciDAC project. The codes employ conformal grids and higher-order finite elements for superior geometry representation and high field accuracy:

- Parallel Finite Element Wakefield Codes T2P, T3P
- Parallel Finite Element PIC Codes Pic2P, Pic3P

Since the 3D PIC code Pic3P is still in development, we will focus on T3P and Pic2P in the following. While T3P is able to accurately calculate transients in accelerating cavities with complex geometries, couplers and boundary conditions, Pic2P is used to simulate space-charge dominated regimes in rotationally symmetric geometries, such as electron guns. This is the first successful implementation of self-consistent particle-field interaction on a conformal, unstructured grid using higher-order Whitney basis functions. Based on 1st principles, the code contains all pertinent physics effects such as space charge, wakefields, and retardation. There is a strong interest in such codes from the RF gun community because of the growing need for high-brightness, low-emittance beams in next-generation free-electron lasers and light sources.

Parallel Implementation

All the time domain codes presented here are written in C++/MPI and use highly optimized iterative or direct sparse linear system solvers on massively parallel architectures. T3P uses domain decomposition and iterative solvers for big problem sizes. Pic2P distributes the macro particles but replicates the system matrix in order to reduce communication costs during the particle pusher field calculation for fastest parallel performance. This is possible in 2D where system sizes are comparably small - which also allows the use of fast direct solvers.

NUMERICAL RESULTS

A majority of our simulation efforts in the past year has turned to accelerator applications such as PEP-II, ILC, LCLS, as well as Advanced Accelerator Concepts. Highlights from these simulations follow.

Wakefield Simulations with T3P

1) Broadband Impedance of PEP-II LER BPM
During PEP-II operation, some beam position monitors (BPM's) in the low-energy ring (LER) lost the buttons due to poor thermal contact. There was a request to find out through simulation the effect of the missing buttons on the ring's broadband impedance. T3P can accurately model the elliptical vacuum chamber and the fine details in the BPM. Fig. 2 shows a high fidelity model of the geometry for the vacuum chamber as well as the BPM with and

without buttons. The mesh resolution had been increased until convergence of the wakefields was found. The results for the short-range wakefields are shown in Fig. 3 which compares the case with buttons to that without buttons indicating the difference is not significant. The PEP-II has since operated normally even with some missing buttons in some LER BPM's.

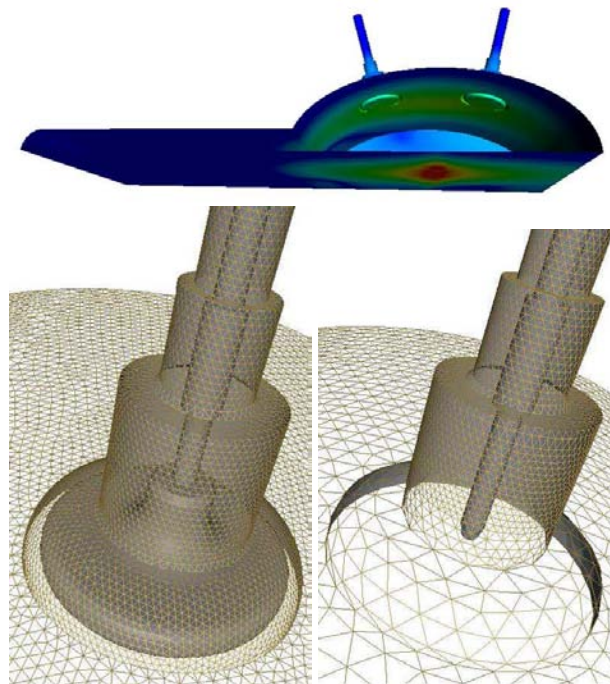


Figure 2: (Top) Upper-half model of PEP-II LER vacuum chamber with two BPM's, showing the beam down the axis, (Bottom) Mesh of BPM with and without button.

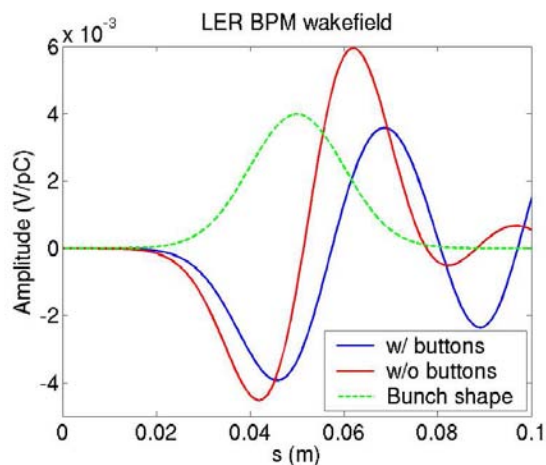


Figure 3: T3P comparison of short-range wakefields in PEP-II LER with and without BPM buttons.

2) The Photon Band Gap (PBG) The PBG is, by design, a single mode structure in which all higher-order

modes (HOM's) are not confined and therefore can escape from the structure once generated by the beam. Massachusetts Institute of Technology (MIT) has fabricated a 17 GHz PBG structure which demonstrated an accelerating field gradient of 35 MV/m in beam tests. The role of simulation is to verify the effectiveness of the PBG concept in damping HOM's. For the MIT 17 GHz structure, both time (T3P) and frequency (Omega3P) domain simulations were carried out, with absorbing boundaries imposed at the outer wall of the PBG structure. One typical HOM computed with Omega3P has a Q_e of 131 and thus is heavily damped. The wakefields excited by an off-axis transit beam modeled with T3P are shown in Fig. 4 where no high fields inside the structure remain after the beam transit, indicating HOM's leak out effectively from the structure.

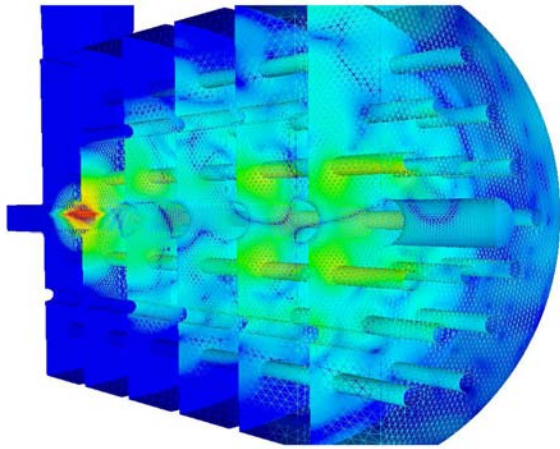


Figure 4: Wakefields in PBG structure generated by off-axis beam, modeled by T3P.

3) ILC TESLA Cavity The temporal electromagnetic field behavior in the ILC TESLA cavity due to a beam transit was simulated with T3P, taking into account the 3D effects from the input and HOM couplers on the short range wakefields. Fig. 5 shows a snapshot in time of the magnetic fields excited by the transiting beam. Performed on

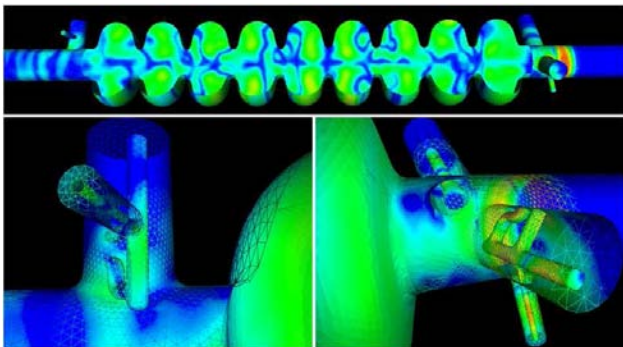


Figure 5: Snapshot of T3P magnetic field contours in ILC TDR cavity and couplers after the beam passes main cavity.

the 'Seaborg' computer at the National Energy Research

Scientific Computing Center (NERSC), the simulation parameters were: 1.75M quadratic elements (10M DOF's), requiring 173 GB on 1024 processors and 47 minutes per nanosecond of beam travel.

LCLS RF Gun Simulations with Pic2P

Simulation Parameters In the following, 2D PIC simulations of the 1.6 cell S-band LCLS RF gun are presented [6]. In the simulations, the gun is driven by the π -mode with an accelerating field gradient of 120 MV/m at the cathode. A uniform, cold, 10 ps long (flat-top) electron bunch of 1 mm radius is emitted from a flat cathode, centered around a phase of -58° with respect to the crest. Bunch charges are varied from zero space charge (10^{-6} nC) up to 1.5 nC.

For Pic2P calculations, a conformal, highly unstructured grid model of the LCLS RF gun is used, with mesh densities concentrated along the beam path, as shown in Fig.6. Second-order elements and basis functions are used, and the cavity modes are obtained to high accuracy with the parallel finite element frequency domain code Omega2P. Although $2^{1/2}$ D treatment of azimuthal dynamics in mag-

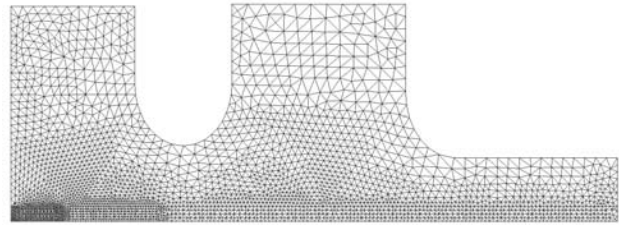


Figure 6: Unstructured 2D grid model of LCLS RF gun.

netostatic fields is fully implemented in Pic2P, solenoid focusing is not included for simplicity. The particle bunch accelerated by the driven cavity mode and the scattered fields generated by the beam in its interaction with the gun cavity are shown in Fig. 7 (Left) and (Right) respectively.

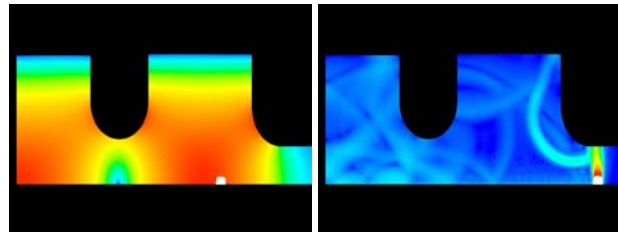


Figure 7: (Left) Particle bunch accelerated by operating mode in LCLS RF gun as simulated with Pic2P, (Right) scattered fields from interactions of bunch with gun cavity.

Code Comparison Comparisons of the RMS bunch radius and the normalized transverse RMS emittance between Pic2P, MAFIA and PARMELA for different bunch charges are shown in Fig. 8. There is excellent agreement

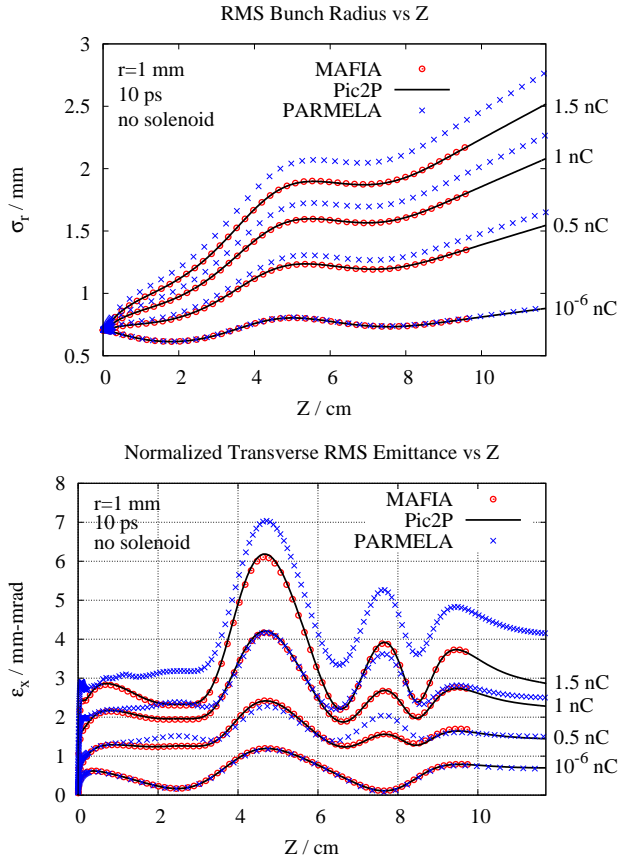


Figure 8: Comparison of RMS bunch radius (Top) and normalized transverse RMS emittance (Bottom) in LCLS RF gun between MAFIA, Pic2P and PARMELA for different bunch charges.

between Pic2P and MAFIA, but PARMELA differs as soon as space charge effects are significant, presumably because it ignores wakefield and retardation effects. The differences can best be seen in a detailed phase space comparison, as shown in Fig. 9.

This is the first time that the wakefields in the LCLS RF gun have been calculated accurately. For a bunch length of 10 ps and 1 nC bunch charge, however, the effect is relatively small, accounting for about a 6% increase in the transverse emittance.

The impact of retardation of the space charge effects is investigated in the following.

Retardation of Space Charge Effects Currently, only Maxwell PIC codes like MAFIA or Pic2P can fully include retarded image and space charge effects in complicated geometries, while electrostatic codes like PARMELA ignore retardation effects and assume instantaneous signal propagation.

In order to compare the instantaneous approximation with the retarded treatment of space charge forces, we consider the longitudinal space charge effect between the tail and the head of a 15 ps long bunch. As can be seen in

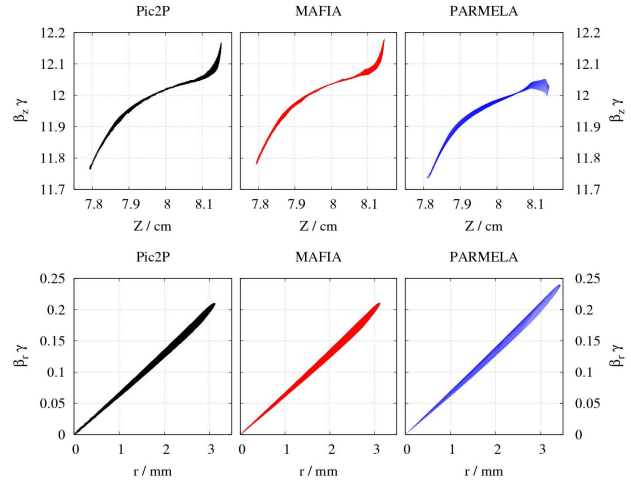


Figure 9: Longitudinal (Top) and transverse (Bottom) phase space comparison between Pic2P, MAFIA and PARMELA in LCLS RF gun for 1.5 nC.

Fig. 10, the forward and backward light cones of the tail, right after its emission, cross the trajectory of the head at two interaction points that are quite different from the instantaneous interaction point, both in space and time. For a

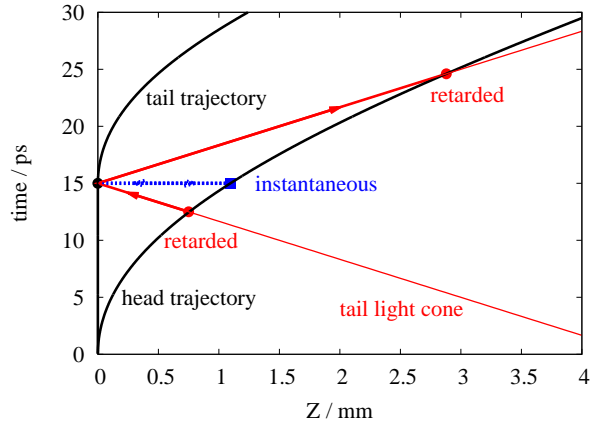


Figure 10: Causality plot for LCLS RF gun with 15 ps long bunch of 1 nC charge. Fully self-consistent head and tail trajectories with retarded head-tail interaction points are compared to corresponding instantaneous signal propagation of electrostatic approximation (PARMELA).

20 ps long bunch, this effect is even stronger: It takes over 40 ps for the tail signal to hit the head at $z=12$ mm. These retardation times (and distances) grow larger and larger as the energy gain per bunch length gets comparable to the particle rest energy.

Retardation not only renders space charge forces non-instantaneous, but also changes their effective impact on the particle dynamics. First, the field amplitude decreases quadratically with the retarded distance, and second, the particles are getting less and less sensitive to space charge forces as they gain on energy, due to magnetic self-

focusing. Thus, the longitudinal space charge forces can be significantly different from the one predicted by the electrostatic approximation.

Performance of Pic2P

Using higher-order particle-field coupling and conformal grids, Pic2P requires far fewer computational resources than MAFIA to reach convergence in the emittance, cf. Fig. 11. The parallel speedup presently achieved

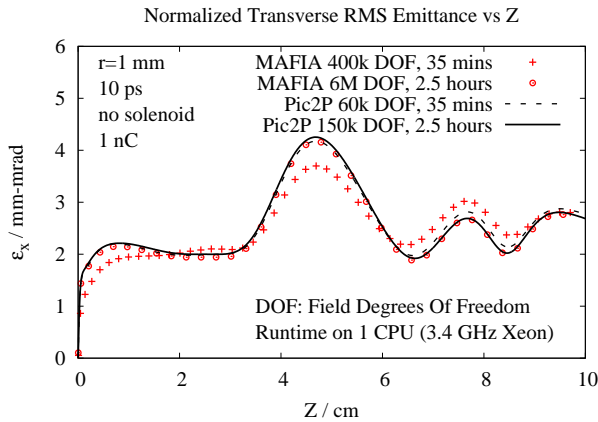


Figure 11: Convergence of normalized transverse RMS emittance in LCLS RF gun for different problem sizes with MAFIA and Pic2P.

by Pic2P, using second-order elements, is shown in Fig. 12. The good scalability makes it viable to use the code as a design tool since the computing time can be reduced to the same order as PARMELA's – only a few minutes – while providing the correct physics model of a self-consistent Maxwell PIC code.

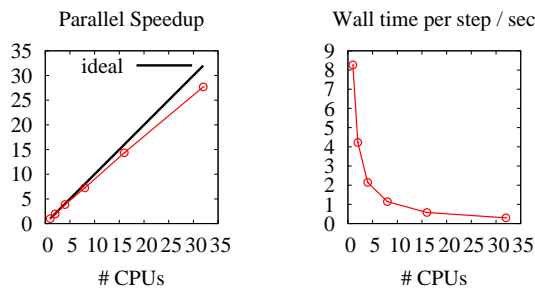


Figure 12: Parallel speedup of Pic2P on NERSC's Linux cluster 'Jacquard'.

CONCLUSIONS AND OUTLOOK

Higher-order finite element methods and parallel processing have enabled electromagnetic field and particle simulations to reach a level of realism and accuracy not previously attainable, and have allowed accelerator applications to progress from single component modeling to simulations at the system scale.

Starting from 1st principles, we have developed parallel finite element time domain codes to study transients and space charge effects in complex accelerator structures. Based on conformal, unstructured grids and higher-order Whitney basis functions with unconditionally stable time-integration, these codes require fewer computational resources to reach convergence than conventional codes based on orthogonal structured grids.

The 3D parallel finite element wakefield code T3P was applied to a broad range of problems to study transient effects in complex cavities such as the ILC, PEP-II and the PBG.

The 2^{1/2}D parallel finite element Maxwell PIC code Pic2P, the first such successful implementation, was used to model the LCLS RF gun. Pic2P shows perfect agreement to MAFIA, while offering faster convergence. Results from the electrostatic code PARMELA differ whenever wakefield and retardation effects are important. This indicates the significance of self-consistent simulation for the design of high-brightness, low-emittance electron guns, for use in next-generation free-electron lasers and light sources.

ACKNOWLEDGMENTS

This work was supported by U. S. DOE contract DE-AC002-76SF00515. This research used resources of the National Energy Research Scientific Computing Center, which is supported by the Office of Science of the U. S. Department of Energy under Contract No. DE-AC02-05CH11231; and of the National Center for Computational Sciences at Oak Ridge National Laboratory, which is supported by the Office of Science of the U. S. Department of Energy under Contract No. DE-AC05-00OR22725. – We also acknowledge the contributions from our SciDAC collaborators in numerous areas of computational science.

REFERENCES

- [1] K. Ko et al., "SciDAC and the International Linear Collider: Petascale Computing for Terascale Accelerator", Invited Talk given at SciDAC 2006 Conference, Denver, Colorado, June 25-29, 2006.
- [2] W. A. Artuzi, "Improving the Newmark Time Integration Scheme in Finite Element Time Domain Methods", IEEE Microwave and Wireless Components Letters, vol. 15, no. 12, December 2005
- [3] N. M. Newmark, "A method of computation for structural dynamics", Journal of Eng. Mech. Div., ASCE, vol. 85, pp. 67-94, July 1959.
- [4] J. P. Boris, "Relativistic plasma simulation-optimization of a hybrid code", Proc. Fourth Conf. Num. Sim. Plasmas, Naval Res. Lab, Wash. D.C., pp. 3-67, Nov. 2-3, 1970.
- [5] O. Buneman, W. Pardo, "Fast numerical procedures for computer experiments on relativistic plasmas", Relativistic Plasmas(The Coral Gables Conference, University of Miami), W. A. Benjamin, New York, pp. 205-219, 1968.
- [6] L. Xiao et al., "Dual Feed RF Gun Design for the LCLS", Proc. PAC 2005, Knoxville, Tennessee, May 15-20, 2005.